

Journal of Mechanics of Materials and Structures

**SHEAR CAPACITY
OF T-SHAPED DIAPHRAGM-THROUGH JOINTS
OF CFST COLUMNS**

Bin Rong, Rui Liu, Ruoyu Zhang, Shuai Liu and Apostolos Fafitis

Volume 12, No. 4

July 2017



SHEAR CAPACITY OF T-SHAPED DIAPHRAGM-THROUGH JOINTS OF CFST COLUMNS

BIN RONG, RUI LIU, RUOYU ZHANG, SHUAI LIU AND APOSTOLOS FAFITIS

Diaphragm-through joints between rectangular concrete-filled steel tubular (CFST) columns and steel beams have been widely used in engineering design. In order to investigate the shear capacity of T-shaped diaphragm-through joints, three such joints were tested under seismic cyclic loading. The test results showed that the main contributors to the shear capacity of the joint are the core concrete and the steel tube. However, the flanges of the steel tube have little effect on the shear capacity. In addition, based on the principle of deformation coordination, a calculation method of shear force-deformation skeleton curve for T-shaped diaphragm-through joints is proposed. The theoretical predictions of the method are well fitted with the experimental results.

1. Introduction

In recent years, concrete-filled steel tubular (CFST) columns have been widely used in practical applications due to their benefits of excellent mechanical behavior and pleasing architectural advantages over conventional columns, particularly in terms of their high strength-to-weight ratio, high flexural stiffness, and aesthetic appearance. Beam to column joints are the main components that transmit loads in the whole structure. Diaphragm-through joints between rectangular CFST columns and steel H-shaped beams have concise form, a clear force transmission mechanism and are easy to install. Thus the diaphragm-through joint has become increasingly popular in high-rise buildings.

A large amount of experimental research and number of theoretical analyses have been conducted on the diaphragm-through joints between CFST columns and steel H-shaped beams [Zhang et al. 2012; Sheet et al. 2013; Qin et al. 2014]. The calculation formula in the AIJ specification [AIJ 1987] proposed by the Architectural Institute of Japan took into account the shear capacity of both the steel tube and the core concrete. The formula was derived directly by superposing the shear capacity of steel and concrete. Fujimoto [2000], Fukumoto and Morita [2005] conducted a series of experiments on the panel zone of internal-diaphragm joints and diaphragm-through joints between CFST columns and steel beams. They proposed the constrained compression truss model of the concrete core. Based on the superposition of shear force-deformation relations for the steel tube and concrete core, a practical calculation method was provided as a trilinear model with a yield strength and an ultimate strength for the panel zone. Lu and Yu [2000] conducted an experiment on five internal-diaphragm joints. The researchers also proposed a formula for the prediction of the yield strength of the joint by superposing the yield strength of each member in the joint, which is derived from the yield line theory. Wu, Chung, Tsai, Lu, and Huang [Wu et al. 2006] conducted a series of cyclic loading experiments on bidirectional bolted beams to CFST

Keywords: CFST column, diaphragm-through joint, shear capacity, experimental research.

column connections. They established a mechanical model to derive theoretical equations for calculating the stiffness, the yielding shear capacity and the ultimate shear capacity of the panel zone. Nie, Qin, and Cai [Nie et al. 2008] conducted a series of cyclic loading experiments on three types of connections inside the frame. Based on the experimental studies, the researchers proposed a calculation method of shear force-deformation skeleton curves by superposition.

Liu et al. [Liu et al. 2014] compared three main calculation methods for the shear capacity of joints between CFST columns and steel beams. The theoretical results were verified with test data. It was found that the applicability of the calculation methods was different between interior and exterior joints. The yield load of exterior joints was significantly nonconservative and the ultimate loads presented scattered results for the existent specimens. The number of exterior joint specimens was small. So further research is needed to develop procedures for accurate assessment of the panel zone shear capacity for exterior joints.

In order to investigate the shear capacity of exterior diaphragm-through joints, three T-shaped joints were tested under seismic cyclic loading in this study. The specimens were designed based on the principle of “strong members and weak joints” to ensure the shear failure in the panel zone of joints. Based on the test results, a nonlinear shear force-deformation model is proposed for the panel zone of exterior diaphragm-through joints between CFST columns and steel beams. This model is verified by experimental results based on various parameters.

2. Experimental design

2.1. Specimen design. Three full-sized T-shaped specimens have been designed to investigate the shear capacity of exterior diaphragm-through joints subjected to seismic cyclic loading. Under seismic actions, story drift occurs in the structure, and the inflection points of beam and column are assumed to occur at the mid-point. The panel zone of the joint is the center of the specimens, and the midpoints of the columns and beams are the boundaries of the specimens. In this T-shaped substructure, three hinges are used to simulate the upper, lower, left or right inflection points to perform the simulation. In order to evaluate the shear capacity of the panel zone, the specimens were designed to be “strong members and weak joints” to ensure the shear failure in the panel zone. This was achieved by making the thickness of the steel tube wall of the panel zone thinner than the ones used in practical engineering.

The thickness of the steel tube wall of the panel zone and diaphragm-through, and the strength of concrete in steel tube are changed for comparison. The dimensions of each specimen are listed in Table 1. Details of panel zone are shown in Figure 1.

Specimen	Column Section (mm)	Beam Section (mm)	Column Section in Panel Zone (mm)	Thickness of Diaphragm (mm)	Concrete
TDTC-1	200 × 200 × 12	H250 × 200 × 8 × 12	200 × 200 × 6	16	C30
TDTC-2			200 × 200 × 6	14	C40
TDTC-3			200 × 200 × 8	14	C30

Table 1. Dimensions of specimens.

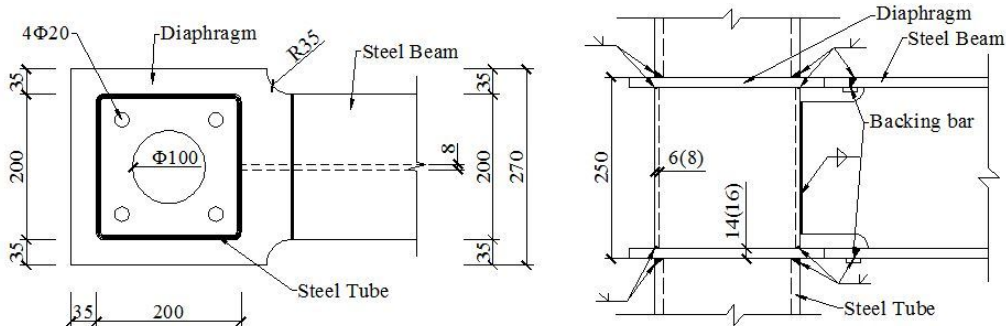


Figure 1. Details of panel zone

Thickness of steel (mm)	f_y (N/mm ²)	f_u (N/mm ²)
6	268.9	387.9
8	249.6	373.1
12	313.8	439.8
14	252.2	414.6
16	250.1	407.3

Table 2. Material properties of steel (f_y is the yield strength and f_u is the tensile strength).

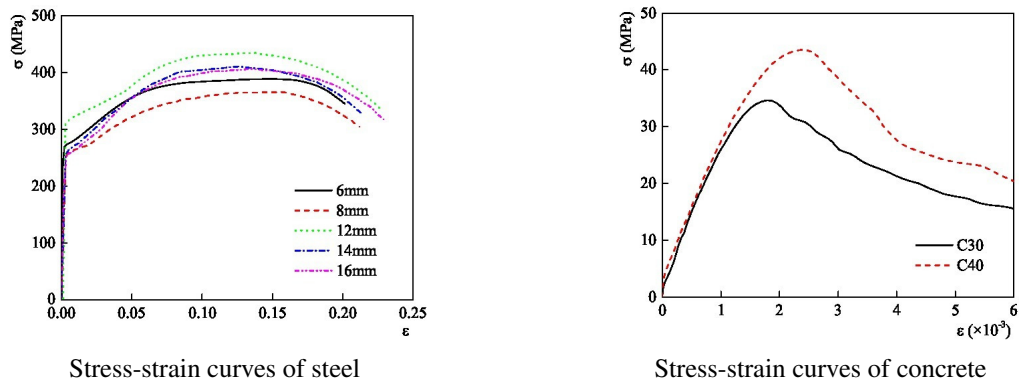
The steel tubes of the specimens were made of cold-formed square steel tube. The beams of the specimens were made of H-shaped steel. The steel tubes were discontinuous at the position of diaphragms, and the diaphragms went through the steel tubes. All the steel components of the joint connected to each other by full penetration butt welds with backing bars. They were processed and welded together in the factory in advance. Then the steel tube was filled with concrete. The specimens were transported to the laboratory after the curing of concrete was completed in the factory.

The strength grade of steel of all the specimens was Q235B. According to the “metallic materials at room temperature tensile test method” (GB/T228-2002), standard tensile pieces of steel from steel tubes and beams of the specimens were cut. The dimension of the tension bar was 180 mm × 40 mm. The material properties of the steel were tested on the universal testing machine, as shown in Figure 2. The stress-strain curves of all thicknesses of steel are shown in Figure 3. The material properties of the steel are listed in Table 2. The grades of concrete in the steel tubes were C30 and C40. According to the “concrete strength inspection and evaluation standards” (GB/T50107-2010), standard concrete test cubes were made when concrete was cast into steel tubes. The dimension of the concrete cubes was 150 mm × 150 mm × 150 mm. The concrete cubes were cured under the same conditions with specimens for 28 days. Compression strength of the concrete cubes was tested on the electrohydraulic universal testing machine, as shown in Figure 2. The stress-strain curves of the two grades of concrete are shown in Figure 3. The material properties of the concrete are listed in Table 3.



Tensile test of steel specimen

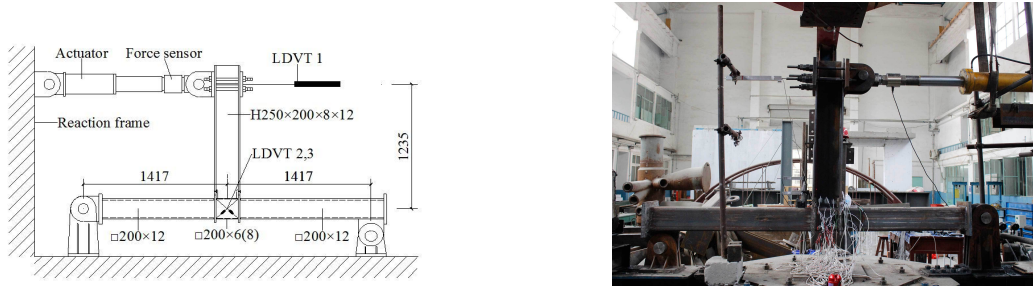
Concrete cube test

Figure 2. Material property test.**Figure 3.** Stress-strain curves of material test results.

Grade of concrete	f_{cu} (N/mm ²)	f'_c (N/mm ²)
C30	34.63	27.36
C40	43.55	34.40

Table 3. Grade of concrete (f_{cu} is the cube compressive strength of concrete and f'_c is the cylinder compressive strength of concrete).

2.2. Test setup and loading procedure. There are two kinds of common loading methods in the joint test, which are loading at the column end and loading at the beam end, respectively. When the research would be affected by the second order effects of gravity on the displacement of the column under horizontal load, the loading at the column end method should be adopted. Since the mechanical properties in the



Schematic drawing of test setup

Photo of test setup

Figure 4. Test setup.

panel zone of the joint will not be influenced by the second order effect of gravity, the beam end loading scheme was adopted in this study. Figure 4 shows the schematic drawing and the photo of the test setup. The T-shaped specimens were placed horizontally on the testing frame first. To simulate the inflection points of the columns and the beams, the T-shaped specimens were fixed on the testing frame by three hinged supports. The displacement of three directions was constrained at the bottom of the column. The top of the column was restricted by the displacement in two directions. The displacement in the direction of the column axis was relaxed, which was achieved by the long hole of the hinged support.

Before the actual experiment, the specimens were preloaded to ensure good contact with the test device. The relationship between load and deformation was stable. The entire test device was reliable. Furthermore, observation equipment worked properly. During the experiment, the horizontal cyclic load at the beam end was controlled by a force-displacement hybrid control loading system. That is, force-control was used before the yielding of the specimen. Displacement-control was employed after the yielding of the specimen. Stepwise force load was applied to the beam end and repeated one time at each step before yielding. After that, the specimen would be controlled by a multiple of the horizontal displacement of the beam end when specimens yielded. This was repeated three times for each step. During the loading process, in order to get the stable deformation data of the joint, the experimental data were collected after keeping the load for 5 minutes per level. The controlled displacement in the loading process was measured by LVDT1 (Linear Variable Differential Transformer), which was placed at the end of the beam corresponding to the location of a horizontal actuator. In addition, the diagonal displacement of the shear panels was measured by LVDT2 and LVDT3, as shown in Figure 4. The measured data were collected by the computer automatically.

2.3. Observations. For the specimen TDTC-1, the thickness of diaphragm was 16 mm. Before yielding, the load-displacement curve was linear. At the load of 139 kN, the joint yielded, while the deformation of the panel zone was so insignificant that no major phenomenon was observed. Beyond this point, the loading continued to increase with the displacement control method. The applied displacements were equal to multiples of yield displacement at the beam end, and the slope of the load-displacement curve became smaller. Local buckling occurred in the steel tube webs of the panel zone during the second cycle in one time of yield displacement. With the increasing displacement of the beam end, the horizontal load kept increasing. The internal force of the specimen was redistributed. The beam flanges began to bear more load transferred from the beam end. Then some local buckling took place on the beam flanges,

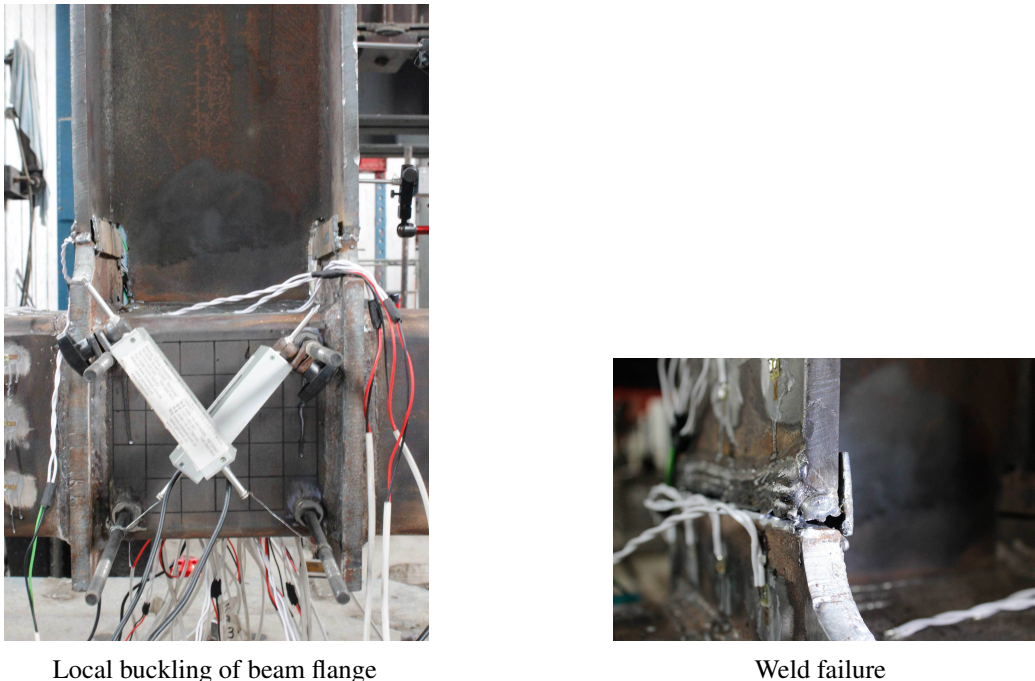


Figure 5. Experimental phenomena of TDTC-1.

as shown in Figure 5. As the load increased, the weld between the steel beam and diaphragm started to fail, as shown in Figure 5. The load reached its peak value of 185.2 kN, corresponding to 50.2 mm displacement. The specimen was then unloaded and the test was terminated. It can be seen that the column web of panel zone bulged outward at the end of the test.

For the specimen of TDTC-2, the grade of filled concrete was C40. At the load of 138 kN, the panel zone yielded and the slope of load-displacement curve became smaller. Then the loading entered into the displacement control stage. TDTC-2 reached its maximum capacity of 199 kN and the corresponding displacement value was 61.1 mm. At four times the yield displacement, some local buckling on the column web of the panel zone became obvious. With the cyclic load at the beam end, the bulging outward of the column web along the two diagonals took place alternately with a characteristic sound. After that, the bearing capacity decreased slowly. At five times the yield displacement, a crack appeared near the weld on the tensile side of the diaphragm. At six times the yield displacement, the crack in diaphragm became bigger, as shown in Figure 6; the bulge outward of column web is shown in Figure 6. The load at the beam end dropped to 163 kN, smaller than 85% of the maximum load, and the test was terminated.

For the specimen of TDTC-3, the thickness of the steel tube in the panel zone was 8 mm. At the load of 160 kN, the panel zone yielded. The rectangular panel zone started to become rhombus at two times of yield displacement. There was a clear deflection of the steel beam due to the deformation of the panel zone, as shown in Figure 7. After the yielding of the panel zone, the internal force of the specimen was redistributed and the beam flanges began to bear more load transferred from the beam end. The TDTC-3 reached its maximum value of 179.3 kN with the corresponding displacement of 37.8 mm. At



Figure 6. Experimental phenomena of TDTC-2.

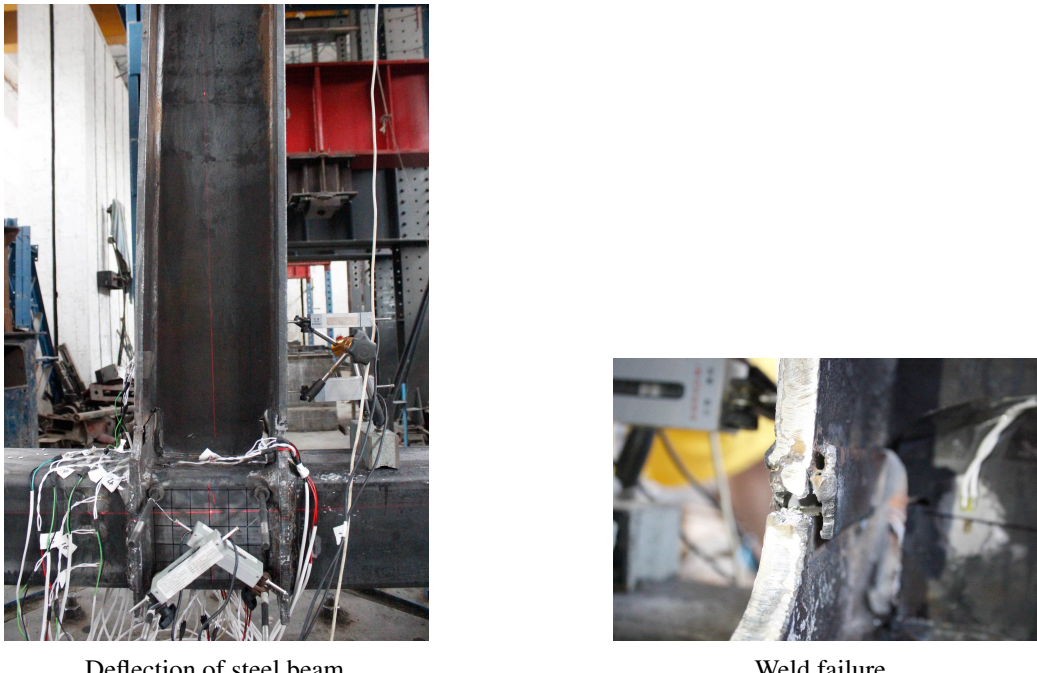
the same time, the weld between the steel beam and diaphragm failed, as shown in Figure 7. The test was terminated.

3. Slitting test of concrete

The steel tube walls at the panel zone of TDTC-2 and TDTC-3 were removed to examine the failure mode of the concrete core of the CFST columns. The distribution of the concrete cracks of TDTC-3 after the panel zone yielded is shown in Figure 8. The severe deformation of the concrete core in the column of TDTC-2 is shown in Figure 8. Under the cyclic load at the beam end, the corner of the panel zone was subjected to tension and pressure transformed from the moment, which was transferred from the beam end and column end. It can be seen from Figure 8 that diagonal cracks appeared and concrete diagonal compression struts formed. According to the test results, it can be found that the width of the diagonal compression strut is about 1/3 of the diagonal length of panel zone.

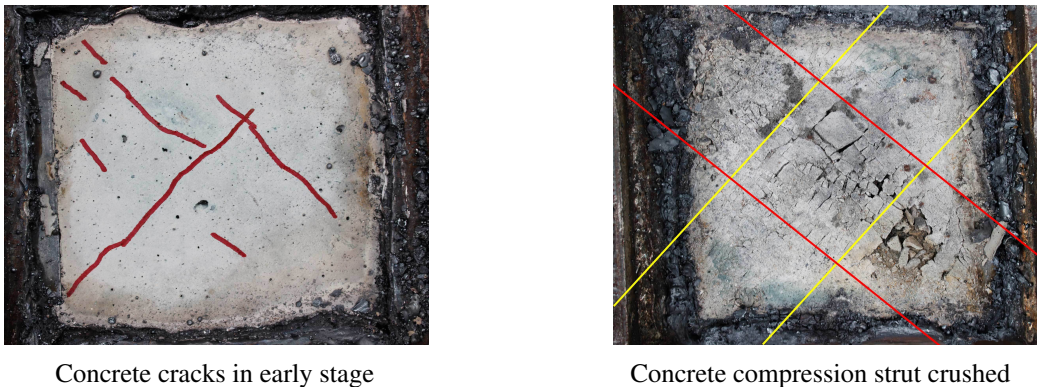
4. Discussion of test results

4.1. Relationships between the shear forces and deformations of panel zone. Shear force-deformation hysteretic curves and skeleton curves of three specimens are shown in Figures 9–11. In these figures, Q is the shear force and γ is the shear deformation of the panel zone. The shape of hysteretic curves of all specimens is smooth and full, which indicates that the specimens have a sound ductile behavior with large energy absorption. The strength decreases gradually after it reaches the maximum point. The slopes of the loading curves of the joints decrease with the increase of the cyclic load. However, the slopes of



Deflection of steel beam

Weld failure

Figure 7. Experimental phenomena of TDTC-3.

Concrete cracks in early stage

Concrete compression strut crushed

Figure 8. Concrete at panel zone.

the unloading curves are almost unchanged, which indicates bigger loading stiffness degradation and smaller unloading stiffness degradation.

The skeleton curves of hysteretic relations, which are obtained through connecting the displacement peaks of all cycles, are shown in Figures 9–11. All the skeleton curves are S-shaped, which indicates that all the specimens have elastic, yielding and hardening stages during the test. In the elastic stage of the joints, shear force-deformation curves are almost straight up. The steel tubes and the concrete are all

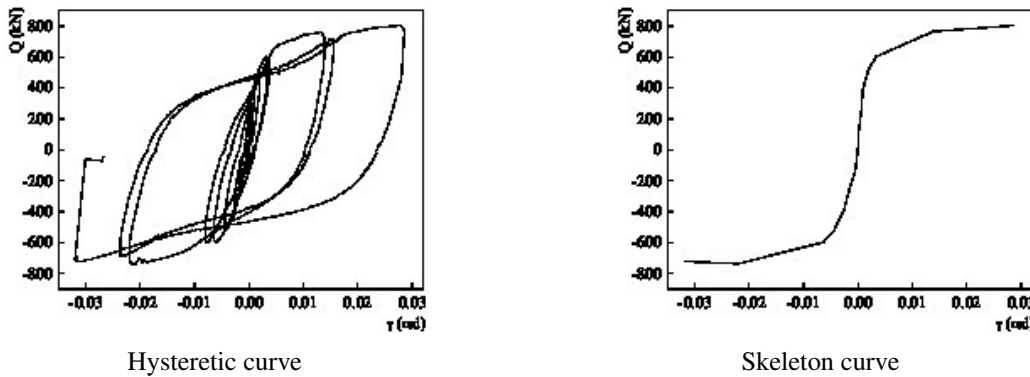


Figure 9. Shear force-deformation of TDTC-1.

in the elastic stage. There are no cracks in the concrete core and the steel tube walls. The concrete and the steel tubes are bonded together effectively. The steel tubes and the concrete can be regarded as an integral part of this stage. The shear stiffness is bigger due to the cooperative working mechanism and deformation joints. In the yielding stage of the joints, the shear deformation increases with the increasing load. The concrete cracks and the web of the steel tube yields. The concrete is separated from the steel tube walls. The slope of shear force-deformation curves declines. Then the web of steel tube enters the hardening phase until it buckles.

After the web of steel tube buckles, the shear resistance of the concrete compression strut increases gradually due to the confinement provided by the steel tube and upper and lower diaphragms. Thus the joints exhibit good ductility. For TDTC-1 and TDTC-3, after the shear yield of the panel zone, the internal forces of the specimen are redistributed, and the beam flanges began to bear more load transferred from beam end. This will lead to the premature failure of the weld between the steel beam and diaphragm. Therefore, the development of shear deformation of the panel zone is insufficient after yielding. The energy dissipation capacity of the panel zone is not fully developed.

The yield shear capacity of specimens is presented in Table 4. From the figures combined with the data of Table 4, it can be seen that the yield shear capacity of TDTC-1 is significantly smaller than that of TDTC-2 and TDTC-3, which indicates that the influence of diaphragm thickness on the shear capacity of the joints is smaller than that of the steel tube wall thickness and the concrete strength. The comparison of TDTC-2 and TDTC-3 demonstrates that the influence of the thickness of steel tube on the shear capacity of the joint is larger.

4.2. Comparison of test results and existing calculation results. In order to evaluate the applicability of the existing calculation methods for the exterior diaphragm-through joints, the results obtained through existing calculation methods are compared with the test results. Three main methods for computing the panel zone shear capacity of composite CFST connections are briefly reproduced here.

4.2.1. Calculation method in [AIJ 1987]. The formula of the method incorporated in AIJ specification is shown in (1). It is derived directly by superposing the shear capacity of the concrete core and the steel tube, where V_c is the volume of the concrete core, f_{JS} is the concrete compression strength (in MPa), β_J is the coefficient for column cross sections, V_s is the volume of the web of the steel tube, and f_y is

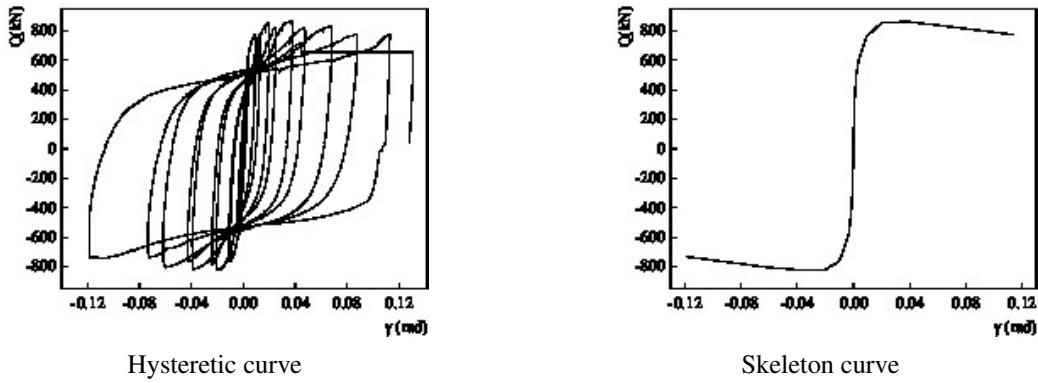


Figure 10. Shear force-deformation of TDTC-2.

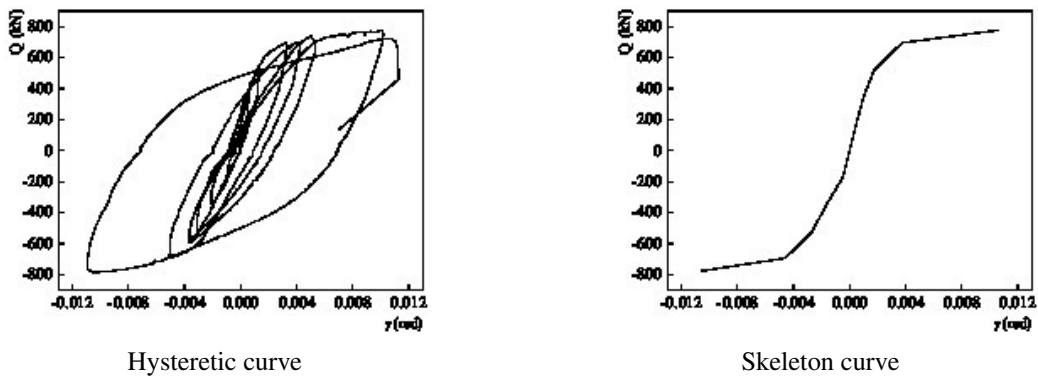


Figure 11. Shear force-deformation of TDTC-3.

the yield tensile strength of the web of steel tube (in MPa).

$$Q = V_c F_{JS} \beta_J + \frac{1.2}{\sqrt{3}} V_s f_y. \quad (1)$$

4.2.2. Calculation method proposed by Lu Xilin (2000). The formula of Lu's method [Lu and Yu 2000] for computing composite panel zone strength is shown in (2), where N_y is the shear capacity of the weld or tube web in the corner, h_c is the width of the cross-section of the concrete core, M_{pw} is the moment of the tube web, M_{pj} is the moment of the inner diaphragm, N_{cv} is the compressive strength of the concrete constrained compression truss, and H_b is the height of the steel beam:

$$Q = (2 N_y h_c + 4 M_{pw} + 4 M_{pj} + N_{cv} h_c / 2) / H_b. \quad (2)$$

4.2.3. Calculation method proposed by Fukumoto and Morita (2005). The formula of Fukumoto's method [Fujimoto et al. 2000] for computing composite panel zone strength is shown in (3), where V_{sy} is the contribution of the shear capacity of the steel tube, V_{cu} is the contribution of the concrete core which is

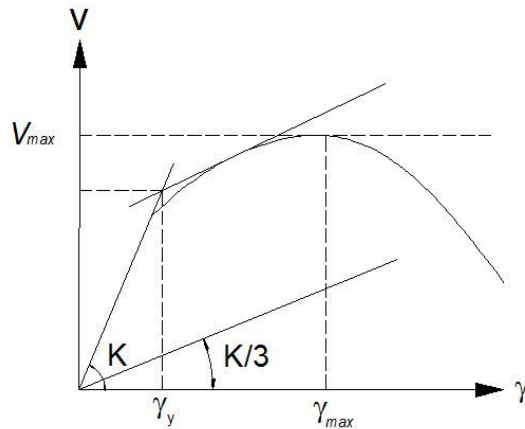


Figure 12. General yield point method.

derived from a constrained compression truss model, and β is the ratio of the shear yield load to shear ultimate load of the concrete core. The shear capacity of the joint is obtained by directly superposing of the contribution of the steel tube and concrete core:

$$Q = V_{sy} + \beta V_{cu}. \quad (3)$$

The comparison of the test results and the existing calculation results of the three T-shaped diaphragm-through joints are shown in Table 4. The yield shear capacity can be obtained by the general yield point method [Park et al. 2010], as shown in Figure 12. The yield point is the intersection point of the two lines, whose slopes are the initial stiffness (K) of the specimen and one-third of the specimen ($K/3$).

It can be seen from Table 4 that the shear capacity of the panel zone increases with the increase of the thickness of the steel tube and the concrete grade. The thickness of diaphragm-through has little influence on the shear capacity of the panel zone. The ratios of the test results and results calculated by AIJ, Lu Xilin, and Fukumoto range from 0.79 to 0.91, 0.70 to 0.77, and 0.97 to 1.17, respectively. They cannot reflect the shear capacity of T-shaped diaphragm-through joints accurately. That is to say, these calculation methods for calculating the shear capacity of panel zone are not suitable for T-shaped diaphragm-through joints. Thus, it is necessary to develop a new shear force-deformation model to estimate the shear capacity of T-shaped diaphragm-through joints accurately.

5. Models for shear force-deformation

5.1. Shear force-deformation of steel tube flange. The rectangular steel tube consists of column flanges and webs. When the beam end is subjected to the horizontal load, shear force is generated in the panel zone. This shear force causes shear deformation at the column web, and flexural deformation at the column flanges, as shown in Figure 13. The shear stiffness and shear capacity of the panel zone are influenced by the shear behavior of the webs and the flexural behavior of the flanges. The shear force

Specimen	Test result Q_e	AIJ		Lui Xilin		Fukumoto	
		Q_y	Q_y/Q_e	Q_y	Q_y/Q_e	Q_e	Q_y/Q_e
TDTC-1	580.65	680.67	0.85	776.53	0.75	529.68	1.09
TDTC-2	638.62	701.78	0.91	828.68	0.77	547.48	1.17
TDTC-3	601.88	763.66	0.79	876.83	0.70	617.39	0.97
<i>Average</i>			0.85		0.74		1.08
<i>Standard deviation</i>			0.049		0.029		0.082

Table 4. Comparison of test and existing calculation results, where Q_e is the shear capacity of the test result and Q_y is the shear capacity calculated with the existing method.

affected by the flexural behavior of the column flanges (V_f) is

$$V_f = K_f \gamma_f, \quad (4)$$

$$K_f = 2 \times \frac{12E_s I}{h_b - 2t_{bf}}, \quad (5)$$

where γ_f is shear strain of the column flanges when it's deformed, E_s is the Young's modulus of steel, h_b is the depth of the H-shaped beam, t_{bf} is the thickness of the diaphragm-through, b_c is the width of the column, t_c is the thickness of the beam flange, K_f is the shear stiffness of the two column flanges due to flexural deformation and $I = b_c t_c^3 / 12$ is the moment of inertia of the column flange.

When the column flanges reach the yielding point, the shear capacity (V_{fy}) is

$$V_{fy} = \frac{4M_{fy}}{h_b - t_{bf}}, \quad (6)$$

where $M_{fy} = b_c t_c^2 f_y / 6$ is the yield flexural strength of the column flanges, and f_y is the yielding tensile stress of the steel. The corresponding shear strain (γ_{fy}) is

$$\gamma_{fy} = \frac{V_{fy}}{K_f}. \quad (7)$$

5.2. Shear force-deformation of steel tube web. The shear force contributed by the shear behavior of the column webs (V_w) is

$$V_w = K_w \gamma_w, \quad (8)$$

where the shear stiffness of column webs before yielding (K_{w1}) is

$$K_{w1} = 2A_w G_s = 2(b_c - t_c)t_c G_s. \quad (9)$$

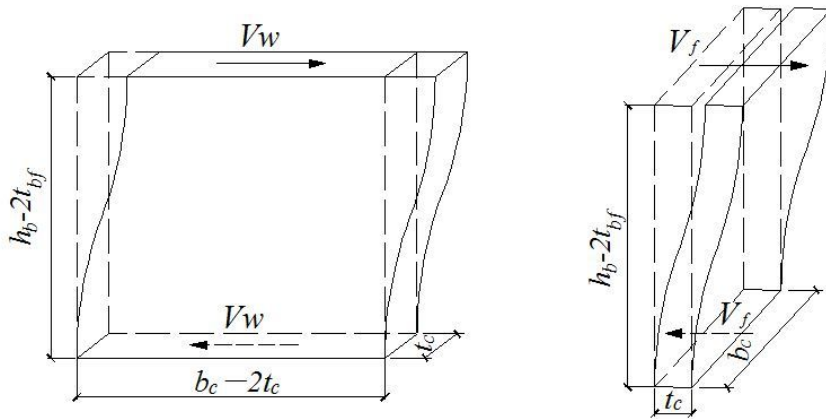


Figure 13. Schematic diagram for deformation of steel tube

When the column webs yield, the strength of the two column webs (V_{wy}) is

$$V_{wy} = 2A_w f_{yv}. \quad (10)$$

The corresponding shear strain of column web (γ_{wy}) is

$$\gamma_{wy} = \kappa \frac{V_{wy}}{K_{wl}} = \kappa \frac{2A_w f_{yv}}{2A_w G_s} = \kappa \frac{f_{yv}}{G_s}, \quad (11)$$

where A_w is the web area of steel tube in the panel zone, $G_s = 79 GP_a$ is the shear modulus for the steel tube and κ is the section coefficient for shear deformation. After reaching the yielding point, the shear stress-strain curve extends continuously at smaller stiffness until the strain is four times the yielding strain due to strain hardening of the material and restraint of the surrounding components [Krawinkler 1978]. Hence, the shear stiffness of the two column webs after yield is

$$K_{w2} = \left(\frac{\beta - 1}{3} \right) K_{w1}, \quad (12)$$

where β is the strain hardening factor, which is the ratio of the ultimate tensile stress to the yield tensile stress.

When the external loads increase continuously, the stress of the column webs subsequently reaches the ultimate point and the strength (V_{wu}) is

$$V_{wu} = 2t_c(b_c - 2t_c) \frac{f_u}{\sqrt{3}}, \quad (13)$$

where f_u is the ultimate tensile stress of the steel.

The corresponding shear strain of column web (γ_{wu}) is

$$\gamma_{wu} = \frac{V_{wu} - V_{wy}}{K_{w2}}. \quad (14)$$

5.3. Shear force-deformation of concrete. For diaphragm-through joints, the concrete compression strut mechanism is activated by the restricting effect of the through-diaphragms and the steel tube wall on

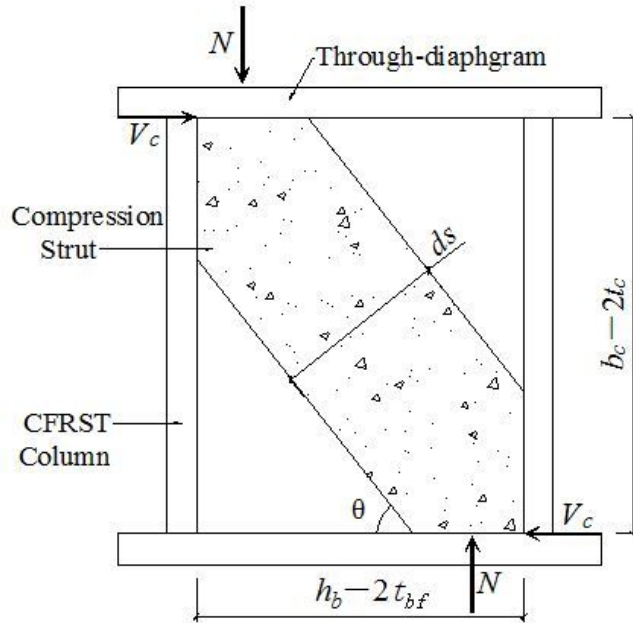


Figure 14. Schematic diagram for concrete compression strut.

the adjacent concrete. The schematic diagram for the concrete compression strut is shown in Figure 14. Based on the analysis in slitting tests of concrete, the concrete compression strut is along the diagonal direction of the panel zone. It is assumed that the width of the compression strut d_s is about 1/3 length of the panel zone diagonal:

$$d_s = \frac{1}{3} \sqrt{(b_c - 2t_c)^2 + (h_b - 2t_{bf})^2}. \quad (15)$$

The angle between the compression strut and the longitudinal beam axis θ is calculated as follows:

$$\theta = \tan^{-1} \frac{b_c - 2t_c}{h_b - 2t_{bf}}. \quad (16)$$

The shear force contributed by the concrete compression strut (V_c) is

$$V_c = f(b_c - 2t_c) \cos \theta, \quad (17)$$

where f is the compression stress of the concrete compression strut.

The stress-strain model for uniaxial and confined concrete under compression, proposed by Samani and Attard [2012], is utilized for the concrete in steel tube columns. This stress-strain model predicts the behavior of normal strength concrete, as well as high strength concrete accounting for the size effects. The complete stress-strain curve is divided into two regions: ascending and descending branches. For the ascending branch,

$$\frac{f}{f_0} = \frac{A \cdot X + B \cdot X^2}{1 + (A - 2)X + (B + 1)X^2}, \quad \text{where } X = \frac{\epsilon}{\epsilon_0} \text{ and } 0 \leq \epsilon \leq \epsilon_0, 0 \leq f \leq f_0. \quad (18)$$

The characteristic values A and B are

$$A = \frac{E_c \epsilon_0}{f_0} \quad \text{and} \quad B = \frac{(A - 1)^2}{0.55} - 1. \quad (19)$$

For the softening descending branch, a power function is used on the condition that the stress-strain curve passes through a point on the softening branch, here taken as the so-called inflection point. The proposed post-peak softening function is

$$\frac{f}{f_0} = \frac{f_r}{f_0} + \left(1 - \frac{f_r}{f_0}\right) \left(\frac{f_{ic}}{f_c}\right)^{\left(\frac{\epsilon_i - \epsilon_0}{\epsilon_i - \epsilon_0}\right)^2}. \quad (20)$$

The inflection point strain ratio is

$$\frac{\epsilon_i}{\epsilon_0} = \left(\frac{f_r}{f_0}\right) \left(1.26 + \frac{2.89}{\sqrt{f'_c}}\right) + \left(1 - \frac{f_r}{f_0}\right) \left(\frac{\epsilon_{ic}}{\epsilon_c}\right). \quad (21)$$

In the above equations, f_0 is the compression strength of confined concrete, ϵ_0 is the corresponding stain, E_c is the secant modulus of concrete, f_r is the residual stress, f_{ic} is the stress level at the inflection point on descending branch of confined concrete, ϵ_{ic} is the corresponding strain and f'_c is the uniaxial compression strength of concrete. Details of the procedure to compute these parameters are described by Samani and Attard [2012].

Actually, compression stress is in one direction diagonally while there is tensile stress acting in the perpendicular direction. This effect should be considered by means of the concrete softening parameter β [Parra-Montesinos and Wight 2001]. The effect of transverse tensile strains on the softening parameter β is a function of the ratio k_{tc} given by $\beta = 1/(0.85 + 0.27k_{tc})$, where k_{tc} is related to the principle tensile and compression strains, with $k_{tc} = -\epsilon_t/\epsilon_c$.

When the concrete core is subjected to the resultant pressure along the diagonal direction, it will deform as Figure 15 shows. According to the relationship between each dimension in the figure, the shear deformation of concrete γ_c can be obtained by the law of cosines through the compression strain ϵ :

$$\gamma_c = \frac{(b_c - 2t_c)^2 + (h_b - 2t_{bf})^2}{(b_c - 2t_c)(h_b - 2t_{bf})} \epsilon. \quad (22)$$

Therefore, the relationship of shear force and deformation for concrete in the panel zone can be determined.

5.4. Models for shear force-deformation of the panel zone. According to the principle of coordination of shear deformation, the shear force-deformation model of the diaphragm-through joints can be obtained through the superposition of models for the steel tube and concrete, given by (23).

$$V_j = V_f + V_w + V_c \quad (23)$$

5.5. Comparison of test and theoretical results. The accuracy of the proposed model to predict the shear force-deformation of T-shaped diaphragm-through joints is evaluated by comparing the predicted versus experimental results, as shown in Figure 16. As these figures show, the proposed model closely predicts the behavior of the joints for all levels of the shear force-deformation curve.

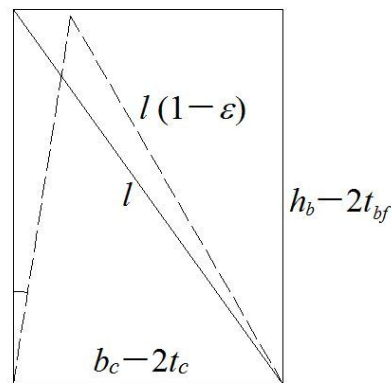


Figure 15. Deformation of concrete core.

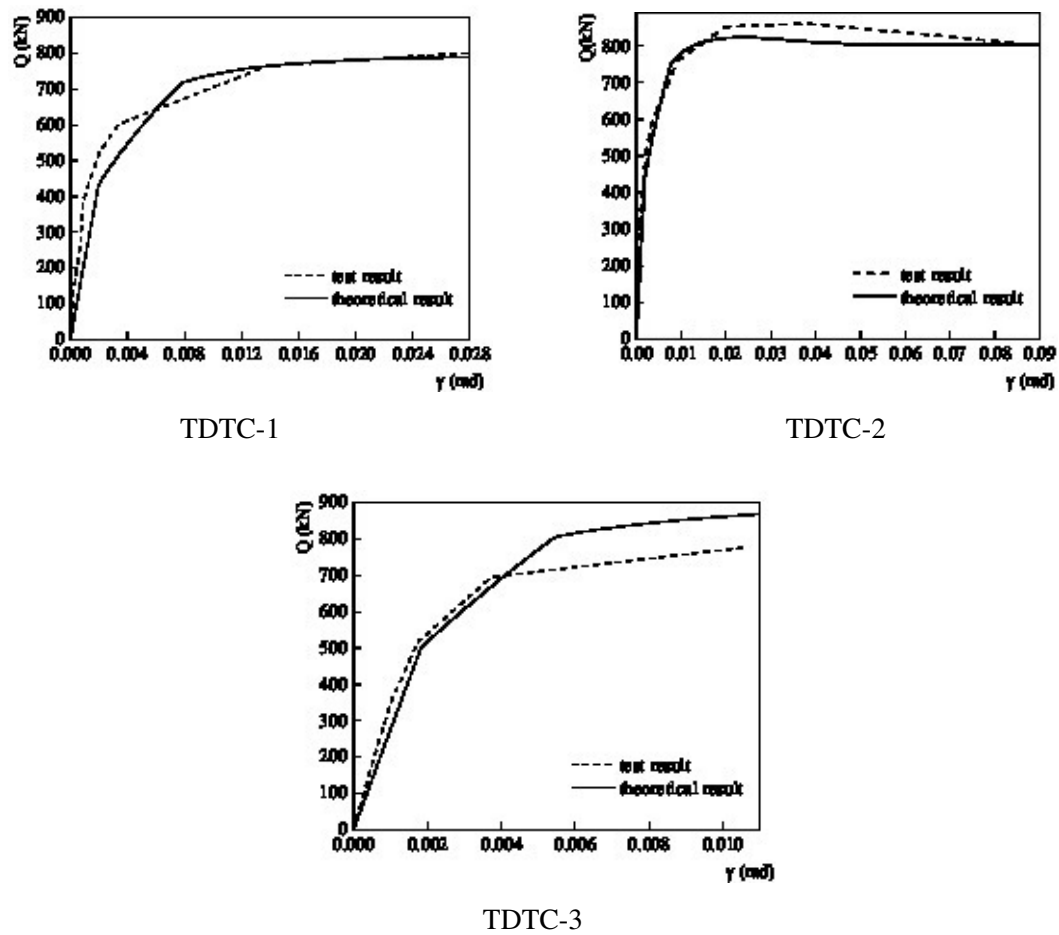


Figure 16. Predicted versus experimental shear force-deformation curves.

Specimen	Q_e	Q_y	Q_y/Q_e
TDTC-1	580.65	609.46	0.953
TDTC-2	638.62	661.54	0.965
TDTC-3	601.88	653.13	0.922

Table 5. Comparison of experimental and theoretical results, where Q_e is the shear capacity of the test result and Q_y is the shear capacity calculated with proposed method.

The predicted results of yield shear capacity for T-shaped diaphragm joints obtained through the proposed model are compared with the experimental results, as shown in Table 5. It can be seen that the theoretical results are in good agreement with the experimental data, the deviation of the prediction results is less than 10%. Because of the premature failure of the weld between the steel beam and diaphragm, the experimental result of TDTC-3 is significantly smaller than the predicted value. The shear force-deformation model proposed in this paper is a valuable tool for predicting the shear capacity of T-shaped diaphragm-through joints.

6. Conclusions

Three T-shaped diaphragm-through joints were tested under seismic cyclic loading to investigate the shear capacity of T-shaped diaphragm-through joints between rectangular CFST columns and H-shaped steel beams. Based on the test results, the following main conclusions are obtained:

- The shear capacity of the T-shaped diaphragm-through joint is contributed by the concrete core and the steel tube, which is composed of webs and flanges. The flanges of the steel tube have little effect on the shear capacity of the joint.
- From the slitting test of the concrete, it is apparent that the concrete compression strut is along the panel zone diagonal direction, and the width of the compression strut is about 1/3 length of the panel zone diagonal.

A model for the shear force-deformation skeleton curve for T-shaped diaphragm-through joints is proposed. The model is developed by superposition of models for steel tubes and the concrete cores based on the principle of deformation coordination. The predictions of the proposed model are in good agreement with the test results.

Acknowledgments

The research described in this paper was financially supported by the National Natural Science Foundations of China (No. 51268054 and No. 51468061) and the Natural Science Foundation of Tianjin City, China (No. 13JCQNJC07300). The financial supports are greatly appreciated.

References

[AIJ 1987] *AIJ standard for structural calculation of steel reinforced concrete structures*, Architectural Institute of Japan, 1987.
In Japanese.

- [Fujimoto et al. 2000] T. Fujimoto, E. Inai, H. Tokinoya, M. Kai, K. Mori, O. Mori, and I. Nishiyama, “Behavior of beam-to-column connection of CFT column system under seismic force”, pp. 557–564 in *Composite and hybrid structures: proceedings of the Sixth ASCCS International Conference on Steel-Concrete Composite Structures* (Los Angeles, 2000), edited by Y. Xiao and S. Mahin, University of Southern California, Los Angeles, 2000.
- [Fukumoto and Morita 2005] T. Fukumoto and K. Morita, “Elastoplastic behavior of panel zone in steel beam-to-concrete filled steel tube column moment connections”, *J. Struct. Eng. (ASCE)* **131**:12 (2005), 1841–1853.
- [Krawinkler 1978] H. Krawinkler, “Shear in beam-column joints in seismic design of steel frames”, *Eng. J.* **15**:3 (1978), 82–91.
- [Liu et al. 2014] X. Liu, M. Tao, J. Fan, and J. Hajjar, “Comparative study of design procedures for CFST-to-steel girder panel zone shear strength”, *J. Constr. Steel Res.* **94** (2014), 114–121.
- [Lu and Yu 2000] X. Lu and Y. Yu, “Experimental study on the seismic behavior in the connection between CFRT column and steel beam”, *Struct. Eng. Mech.* **9**:4 (2000), 365–374.
- [Nie et al. 2008] J. Nie, K. Qin, and C. Cai, “Seismic behavior of connections composed of CFSSTCs and steel-concrete composite beams—experimental study”, *J. Constr. Steel Res.* **64**:10 (2008), 1178–1191.
- [Park et al. 2010] S. Park, S. Choi, Y. Kim, Y. Park, and J. Kim, “Hysteresis behavior of concrete filled square steel tube column-to-beam partially restrained composite connections”, *J. Constr. Steel Res.* **66**:7 (2010), 943–953.
- [Parra-Montesinos and Wight 2001] G. Parra-Montesinos and J. Wight, “Modeling shear behavior of hybrid RCS beam-column connections”, *J. Struct. Eng. (ASCE)* **127**:1 (2001), 3–11.
- [Qin et al. 2014] Y. Qin, Z. Chen, and B. Rong, “Component-based mechanical models for axially-loaded through-diaphragm connections to concrete-filled RHS columns”, *J. Constr. Steel Res.* **102** (2014), 150–163.
- [Samani and Attard 2012] A. Samani and M. Attard, “A stress-strain model for uniaxial and confined concrete under compression”, *Eng. Struct.* **41** (2012), 335–349.
- [Sheet et al. 2013] I. Sheet, Gunasekaran, U., and G. MacRae, “Experimental investigation of CFT column to steel beam connections under cyclic loading”, *J. Constr. Steel Res.* **86** (2013), 167–182.
- [Wu et al. 2006] L.-Y. Wu, L.-L. Chung, S.-F. Tsai, C.-F. Lu, and G.-L. Huang, “Seismic behavior of bidirectional bolted connections for CFT columns and H-beams”, *Eng. Struct.* **29**:3 (2006), 395–407.
- [Zhang et al. 2012] D. Zhang, S. Gao, and J. Gong, “Seismic behavior of steel beam to circular CFST column assemblies with external diaphragms”, *J. Constr. Steel Res.* **76** (2012), 155–166.

Received 2 May 2016. Revised 8 Oct 2016. Accepted 12 Oct 2016.

BIN RONG: tjerobin@126.com

Key Laboratory of Coast Civil Structure Safety, Department of Civil Engineering, Tianjin University, Tianjin, 300072, China

RUI LIU: liurui5919@163.com

Department of Civil Engineering, Tianjin University, Tianjin, 300072, China

zryu@163.com

RUOYU ZHANG: zryu@163.com

School of Civil Engineering, Tianjin University, Weijin Road 92, Tianjin, 300072, China

SHUAI LIU: lao_xs@163.com

Department of Civil Engineering, Tianjin University, Tianjin, 300072, China

APOSTOLOS FAFITIS: fafitis@asu.edu

Department of Civil and Environmental Engineering, Arizona State University, Tempe, AZ 85287, United States

JOURNAL OF MECHANICS OF MATERIALS AND STRUCTURES

msp.org/jomms

Founded by Charles R. Steele and Marie-Louise Steele

EDITORIAL BOARD

ADAIR R. AGUIAR	University of São Paulo at São Carlos, Brazil
KATIA BERTOLDI	Harvard University, USA
DAVIDE BIGONI	University of Trento, Italy
YIBIN FU	Keele University, UK
IWONA JASIUK	University of Illinois at Urbana-Champaign, USA
IMITSUTOSHI KURODA	Yamagata University, Japan
C. W. LIM	City University of Hong Kong
THOMAS J. PENCE	Michigan State University, USA
GIANNI ROYER-CARFAGNI	Università degli studi di Parma, Italy
DAVID STEIGMANN	University of California at Berkeley, USA
PAUL STEINMANN	Friedrich-Alexander-Universität Erlangen-Nürnberg, Germany

ADVISORY BOARD

J. P. CARTER	University of Sydney, Australia
D. H. HODGES	Georgia Institute of Technology, USA
J. HUTCHINSON	Harvard University, USA
D. PAMPLONA	Universidade Católica do Rio de Janeiro, Brazil
M. B. RUBIN	Technion, Haifa, Israel

PRODUCTION production@msp.org

SILVIO LEVY Scientific Editor

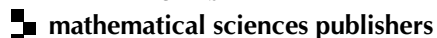
Cover photo: Mando Gomez, www.mandolux.com

See msp.org/jomms for submission guidelines.

JoMMS (ISSN 1559-3959) at Mathematical Sciences Publishers, 798 Evans Hall #6840, c/o University of California, Berkeley, CA 94720-3840, is published in 10 issues a year. The subscription price for 2017 is US \$615/year for the electronic version, and \$775/year (+\$60, if shipping outside the US) for print and electronic. Subscriptions, requests for back issues, and changes of address should be sent to MSP.

JoMMS peer-review and production is managed by EditFLOW® from Mathematical Sciences Publishers.

PUBLISHED BY



mathematical sciences publishers

nonprofit scientific publishing

<http://msp.org/>

© 2017 Mathematical Sciences Publishers

Journal of Mechanics of Materials and Structures

Volume 12, No. 4

July 2017

B-splines collocation for plate bending eigenanalysis

CHRISTOPHER G. PROVATIDIS 353

Shear capacity of T-shaped diaphragm-through joints of CFST columns

BIN RONG, RUI LIU, RUOYU ZHANG, SHUAI LIU and APOSTOLOS FAFITIS 373

Polarization approximations for elastic moduli of isotropic multicomponent materials

DUC CHINH PHAM, NGUYEN QUYET TRAN and ANH BINH TRAN 391

A nonlinear micromechanical model for progressive damage of vertebral trabecular bones

EYASS MASSARWA, JACOB ABOUDI,
FABIO GALBUSERA, HANS-JOACHIM WILKE and RAMI HAJ-ALI 407

Nonlocal problems with local Dirichlet and Neumann boundary conditions

BURAK AKSOYLU and FATIH CELIKER 425

Optimization of Chaboche kinematic hardening parameters by using an algebraic method based on integral equations

LIU SHIJIE and LIANG GUOZHU 439

Interfacial waves in an A/B/A piezoelectric structure with electro-mechanical imperfect interfaces

M. A. REYES, J. A. OTERO and R. PÉREZ-ÁLVAREZ 457

Fully periodic RVEs for technological relevant composites: not worth the effort!

KONRAD SCHNEIDER, BENJAMIN KLUSEMANN and SWANTJE BARGMANN 471

Homogenization of a Vierendeel girder with elastic joints into an equivalent polar beam

ANTONIO GESUALDO, ANTONINO IANNUZZO, FRANCESCO PENTA
and GIOVANNI PIO PUCILLO 485

Highly accurate noncompatible generalized mixed finite element method for 3D elasticity problems

GUANGHUI QING, JUNHUI MAO and YANHONG LIU 505

Thickness effects in the free vibration of laminated magnetoelectroelastic plates

CHAO JIANG and PAUL R. HEYLIGER 521

Localized bulging of rotating elastic cylinders and tubes

JUAN WANG, ALI ALTHOBAITI and YIBIN FU 545

